Journal of Hydrology 666 (2026) 134858

Contents lists available at ScienceDirect

Journal of Hydrology

journal homepage: www.elsevier.com/locate/jhydrol

Research papers

Tracking drought-flood abrupt alternations: Event identification, path analysis, and ecological impacts on vegetation

Xiaoyan Bai [a], Yue Yao [a], Jiefeng Wu [b,*], Yulei Xie [c,*], Zhenxing Zhang [d]

[a] Guangzhou Key Laboratory of Environmental Catalysis and Pollution Control, Guangdong Key Laboratory of Environmental Catalysis and Health Risk Control, School of Environmental Science and Engineering, Institute of Environmental Health and Pollution Control, Guangdong University of Technology, Guangzhou 510006, China
[b] College of Civil Engineering, Hefei University of Technology, Hefei, China
[c] School of Ecology, Environment and Resources, Guangdong University of Technology, Guangzhou 510006, China
[d] Illinois State Water Survey, Prairie Research Institute, University of Illinois at Urbana-Champaign, 2204 Griffith Drive, Champaign, IL 61820, USA

ARTICLE INFO

This manuscript was handled by Dr Marco Borga, Editor-in-Chief, with the assistance of Luca Brocca, Associate Editor

Keywords:
Drought-flood abrupt alternation
Three-dimensional identification
Response
Vegetation

ABSTRACT

Drought-flood abrupt alternation (DFAA) is a regional phenomenon characterized by spatiotemporal propagation continuity within the climate system's dynamic evolution. Previous studies have typically examined the temporal or spatial dimensions of DFAA in isolation, overlooking its inherent spatiotemporal continuity and ecological consequences. This study proposes a novel three-dimensional identification method for drought-to-flood (DTF) and flood-to-drought (FTD) events in the Pearl River Basin. Key spatiotemporal features—duration, area, intensity, centroid, and migration direction—are quantified, and vegetation responses are evaluated using anomalies in fractional vegetation cover (FVC), normalized difference vegetation index (NDVI), and net primary productivity (NPP). The method proves highly applicable, identifying 47 DTF and 52 FTD events during 1979–2018. Among these, 41 DTF and 39 FTD events migrated predominantly westward. DTF events showed longer migration durations (mean: 4.7 months) and larger affected areas (mean coverage: 66 %) than FTD events (4.0 months; 57 % coverage). Spatiotemporal centroids were concentrated in the central basin from February to April for DTF and July to September for FTD. Vegetation response was characterized by rapid FVC/NDVI reaction to DTF (1–2 months lag) but delayed response to FTD (6–8 months lag), whereas NPP showed consistently low sensitivity with a 7-month lag to both. DTF exerted stronger inhibition on vegetation than FTD; over time, FVC/NDVI suppression weakened, while NPP displayed increasingly positive responses. This study provides a new approach for analyzing DFAA evolution and reveals distinct vegetation response mechanisms.

1. Introduction

Drought and flood disasters are the most common natural disasters, causing approximately $40 billion in economic losses to global economy each year (Gao et al., 2019). Meanwhile, climate change, by accelerating hydrological cycles and inducing droughts and floods with higher frequency and stronger intensity, has also increased the risk of more frequent and intense Drought-Flood Abrupt Alternation (DFAA) events (Gao et al., 2022; Hirabayashi et al., 2010; Rahmani and Fattahi, 2023; Tan et al., 2023). As a composite disaster, a DFAA event depicts the abrupt transition between drought and flood conditions within a brief timeframe, forming a typical disaster chain derived from the rapid succession of these two extreme meteorological hazards (Wu et al., 2006; Zhao et al., 2020; Zhou et al., 2023). These events often cause greater harm to both human society and the environment, such as overwhelming water management systems, devastating crop yields, and triggering secondary disasters like landslides, compared to single drought or flood events (Zhang and Wang, 2022). Therefore, studying the dynamics of DFAA events and their impacts on the ecological system is of great significance for disaster prevention and mitigation.

In recent years, growing scientific attention has focused on DFAA events, driving significant methodological advancements in their identification. To accurately identify these events, various indices have been constructed, such as the long-cycle DFAA index (LDFAI), standardized drought-wetness abrupt alternation index (SDWAI), and daily-scale dry-wet abrupt alternation index (DWAAI), among others (Ren et al., 2023; Shan et al., 2018; Tu et al., 2022). These indices have evolved to cover different time scales, ranging from seasonal and monthly scales to daily

* Corresponding authors.
E-mail addresses: wujf27@hfut.edu.cn (J. Wu), xieyulei001@gmail.com (Y. Xie).

https://doi.org/10.1016/j.jhydrol.2025.134858
Received 26 July 2025; Received in revised form 26 November 2025; Accepted 24 December 2025
Available online 25 December 2025
0022-1694/© 2025 Elsevier B.V. All rights are reserved, including those for text and data mining, AI training, and similar technologies.

assessments. Additionally, the intensity and speed of alternation have been defined, and the accuracy of DFAA event recognition is continuously improving (Wang et al., 2021a; Wang et al., 2024b; Yu et al., 2024). While these indices have advanced DFAA identification, most are based on a single meteorological or hydrological variable and thus may not fully capture the complex interactions between atmospheric and terrestrial water processes during DFAA events (Rezvani et al., 2023; Tabari et al., 2021). Therefore, in this study, we select the multi-factor standardized DFAA index (MSDFI). The MSDFI is uniquely suited for this study as it integrates these three key variables—precipitation, evapotranspiration, and soil moisture—across multiple temporal scales using a copula function (Bai et al., 2024). This multivariate and multi-scale framework makes the MSDFI particularly suitable for robustly identifying DFAA events and enables an in-depth investigation into the dynamic evolution processes of both drought to flood (DTF) and flood to drought (FTD) transitions.

Following the identification of DFAA events, researchers have primarily focused on analyzing their temporal and spatial distribution, as well as their evolution (Shi et al., 2021; Zhao et al., 2022). For example, Su et al. (2024) employed the entropy weighting method to determine the intensity characteristics of daily DFAA events, analyzing the temporal and spatial distribution, as well as the development trends in the frequency and intensity of DFAA events across mainland China. Liu et al. (2023), using DFAA events identified through streamflow data, developed a DFAA risk assessment model to assess the intensity, frequency and risk of DFAA events in the Dianchi Basin, highlighting their spatial and temporal differences. Bi et al. (2023) compared the spatial coverage and frequency of DFAA events across 10 Chinese watersheds of varying ages, utilizing the proposed multi-indicator daily DFAA determination method. While these studies have advanced the understanding of DFAA events, they typically treat spatial and temporal dimensions in isolation (Cui et al., 2025; Nie et al., 2025; Yang et al., 2022). However, DFAA is inherently a continuous and dynamic process that evolves simultaneously in both space and time. Analyzing these dimensions separately may overlook the integrated spatiotemporal behavior and migration pathways of events. Therefore, to comprehensively capture the full life cycle and dynamic evolution of DFAA events, this study adopts a three-dimensional method. This approach allows for a holistic analysis of event duration, spatial extent, and trajectory within a unified structure, providing deeper insights into the connected nature of DFAA processes.

In the field of three-dimensional spatio-temporal research, numerous scholars have made pioneering contributions to understanding the dynamic evolution mechanisms of natural disaster events. Li et al. (2022a) developed a spatio-temporal analysis method. Specifically, this method integrates the three-dimensional features of time, latitude, and longitude to analyze the spatial distribution and evolution characteristics of the dry-wet structures in the Huai River basin. However, they did not further analyze the spatial–temporal migration paths of wet-dry alternation events. Compared to conventional two-dimensional methods that primarily examine spatial distribution or temporal variation in isolation, the three-dimensional spatio-temporal analysis method offers significant advantages in capturing the continuous evolution of disaster events. This approach enables the identification of complete event trajectories, which are essential for understanding the dynamic behavior of DFAA events. Recent studies have demonstrated the efficacy of this method in delineating the migratory pathways of drought events (Li et al., 2025; Wang et al., 2024a; Yang et al., 2024; Yang et al., 2025). For example, Feng et al. (2024) established a three-dimensional parameter system containing trajectory, direction and distance from the perspective of propagation of meteorological drought to agricultural drought. The three-dimensional spatio-temporal analysis method has proven to be an effective tool for tracking the spatio-temporal propagation trajectory of disaster events. It provides novel research that enables a deeper understanding of the evolution mechanism of DFAA events.

Moreover, the impacts of DFAA events on vegetation have thus far received relatively little attention, despite their critical significance for ecosystem stability and agricultural security. Most existing studies have focused on the consequences of individual drought or flood events. However, the ecological ramifications of DFAA are likely to be more severe and complex than those of isolated extremes, as vegetation is subjected to successive hydrological stresses under rapidly alternating conditions (Huang et al., 2019; Qian et al., 2023; Xiong et al., 2020; Zhu et al., 2020). For instance, Xiong et al. (2019) discovered that DFAA events led to a greater reduction in rice yield than a single drought or flood event. Similarly, Liu et al. (2024) found that the impact of prior drought on rice physiology during DFAA events depended on its intensity. A subsequent flood had an antagonistic effect following mild drought but synergistically exacerbated the damage after moderate or severe drought. However, it should be noted that drought and flood events are not stationary. The research approach mentioned above, which depends on planting experiments, has limitations: it is restricted to specific regions and subjects. Consequently, it is difficult to fully reveal the impacts of DFAA events across different spatial and temporal scales.

The rapid advancement of satellite remote sensing technology in recent years has provided crucial technical support for the dynamic monitoring of the physiological state of disaster-affected vegetation across various spatial and temporal scales. Remote sensing vegetation indices, such as solar-induced chlorophyll fluorescence (SIF) and the normalized difference vegetation index (NDVI), have been used to study the impact of DFAA events on vegetation across long time series and large spatial scales (Shi et al., 2022; Shi et al., 2024). However, different vegetation traits exhibit varying responses to drought and flood disasters, and a single vegetation index is insufficient to fully analyze the impacts of DFAA events (Wang et al., 2021b; Wang et al., 2025b). Therefore, this study will utilize NDVI, fractional vegetation cover (FVC), and net primary productivity (NPP) to investigate the effects of DFAA events. Among them, the NDVI, by measuring the ratio of near-infrared to red light wavelengths, provides a robust measure of vegetation greenness, photosynthetic activity, and biomass conditions (Huang et al., 2020). The FVC quantifies the proportion of the vertical projection area of vegetation to the unit area, directly reflecting the spatial extent of vegetation canopy and describing the spatial distribution of vegetation cover (Yan et al., 2022). The NPP reflects the ability of plants to fix atmospheric carbon through photosynthesis and convert it into biomass, serving as an essential indicator of carbon sequestration capacity and ecosystem productivity (Chen et al., 2021). By using multiple representative vegetation indices, the impact of DFAA events on the vegetation ecosystem can be more comprehensively revealed.

This study takes the Pearl River Basin, the largest river basin in southern China and the location of the Guangdong-Hong Kong-Macao Greater Bay Area-one of China's most economically dynamic regions-as a case to conduct relevant research, with the goal of enhancing regional disaster prevention and mitigation capabilities and safeguarding sustainable economic development. This study proposes a method for identifying three-dimensional DFAA events and evaluates their impact on the vegetation ecosystem. First, identify DFAA events using a three-dimensional clustering algorithm. Then, analyze the spatiotemporal characteristics of DFAA events, including duration, area, intensity, spatiotemporal centroid, and migration direction. Finally, examine the changes in vegetation indices in the affected areas during each DFAA event and determine the response time of different vegetation indices to these transitions. The findings will deepen the understanding of the dynamic evolution of DFAA events and their impacts on vegetation, thereby contributing to the realization of the aforementioned research objectives.

2. Materials and methods

2.1. Study area and data

2.1.1. Study area

The Pearl River Basin (21°31′–26°49′N, 102°14′–115°53′E), located in southern China, is one of the world's most significant river systems (Fig. 1). The Pearl River Basin (PRB) is the largest river basin in southern China, and its lower reaches form the Pearl River form the Guangdong-Hong Kong-Macao Greater Bay Area, which is currently the most economically dynamic region in China (one of the world's most renowned bay areas). As a globally representative humid climate zone, it features complex geographical conditions and distinctive hydrological characteristics. The PRB is dominated by a monsoon-influenced climate, encompassing an area of approximately 453,690 km^2, with an annual precipitation ranging from 1,500 to 2,400 mm (Zhang et al., 2018). Its diverse topography, spanning from mountainous regions to plains, coupled with dense vegetation sustained by warm and humid climatic conditions, makes the PRB a critical area for studying global climate change and hydrological extremes.

2.1.2. Meteorological and soil moisture data

This study employs the standardized deficit moisture index (SDMI) to quantify drought and flood conditions. The SDMI is constructed by integrating the standardized precipitation evapotranspiration index (SPEI) and the standardized soil moisture index (SSMI). The SPEI is derived from the water deficit/surplus series (precipitation minus potential evapotranspiration). A suitable probability distribution is fitted to the series, and the cumulative probability is then transformed into a standardized index using the inverse standard normal distribution. Similarly, the SSMI is obtained by fitting an appropriate distribution to the soil moisture data and applying the same normalization procedure. Meteorological data for calculating SPEI were obtained from the China Meteorological Forcing Dataset (CMFD) developed by Tsinghua University, which covers the period from January 1979 to December 2018 with a spatial resolution of 0.1° and a temporal resolution of 3 h (He et al., 2020). Soil moisture data for SSMI were derived from the ERA5-Land reanalysis dataset provided by the European Centre for Medium-Range Weather Forecasts (ECMWF), featuring a spatial resolution of 0.1° and a monthly temporal resolution (Muñoz-Sabater et al., 2021).

2.1.3. Remote sensing vegetation data

To assess the ecological impacts of DFAA events on vegetation, three remote sensing vegetation parameters were utilized: FVC, NPP, and NDVI. FVC and NPP data were obtained from the Global Land Surface Satellite (GLASS) products, developed by the College of Global Change and Earth System Science at Beijing Normal University (Liang et al., 2021). These products are generated through multi-source remote sensing data fusion and optimized using machine learning algorithms, and they are widely recognized within the international Earth observation community (Jia et al., 2019; Yu et al., 2018). The GLASS dataset spans from January 1982 to December 2018 with an 8-day temporal resolution and a spatial resolution of 0.05°. NDVI data were acquired from the Peking University Global Inventory Modeling and Mapping Studies NDVI (PKU GIMMS NDVI) dataset, which addresses sensor radiometric degradation and volcanic aerosol interference in Advanced Very High-Resolution Radiometer (AVHRR) data, making it suitable for long-term vegetation monitoring (Li et al., 2023). The PKU GIMMS NDVI dataset covers January 1979 to December 2018 with a biweekly temporal resolution and a 1/12° spatial resolution. The FVC and NDVI datasets were temporally aggregated to a monthly scale using the maximum value composite method to minimize the impact of clouds and atmospheric contamination. The monthly NPP data were synthesized using an accumulation method to represent the total productivity over each month. All datasets were spatially resampled to a 0.1° resolution via bilinear interpolation to ensure consistency in the analysis.

2.1.4. Land use data

The land cover classification data were sourced from the "Annual 30-m Land Cover Dataset of China (1985–2023)" (Yang and Huang, 2021).

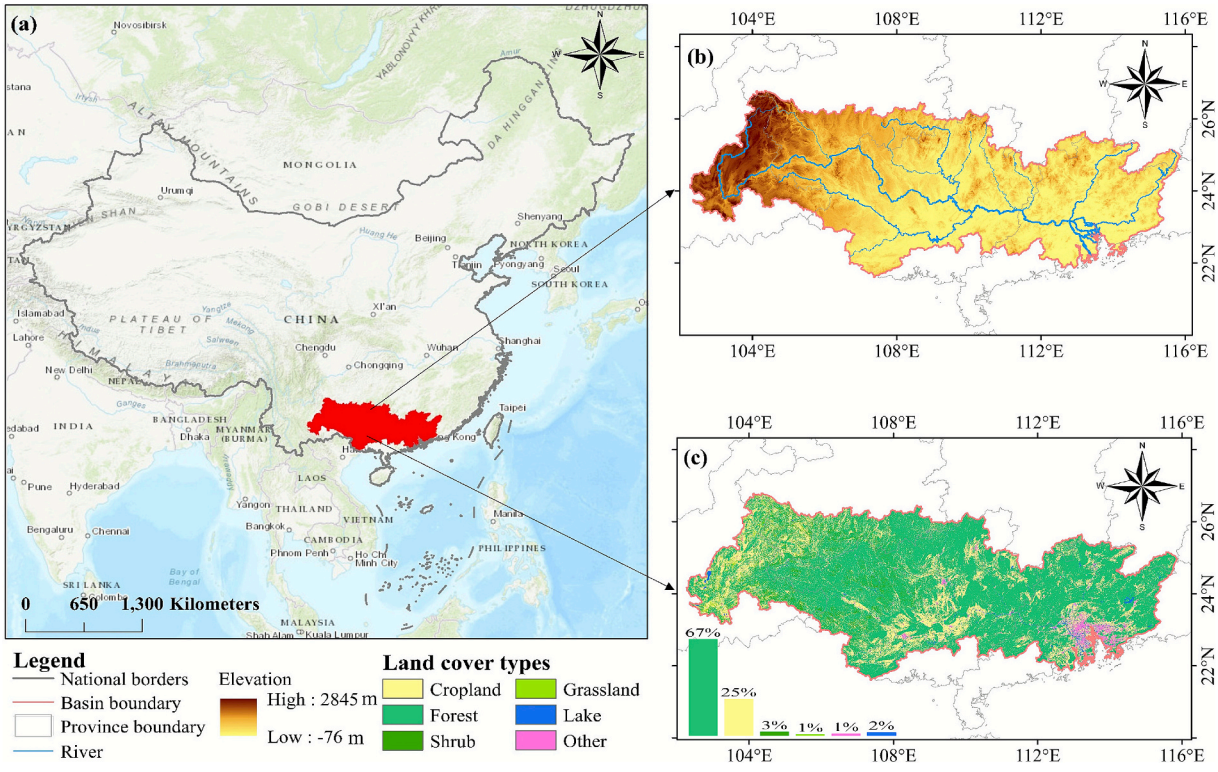


Fig. 1. Location of the study area. (a) Thumbnail map of the study area in China. (b) Map of the Pearl River Basin elevation system. (c) Map of land cover types.

The 2018 data from this dataset, which provides spatial classifications of a 30-meter resolution, were used in this study. Four land cover types—cropland, forest, shrub, and grassland—were selected to discuss land-use patterns associated with vegetation dynamics. The data sources are listed in Table 1.

2.2. Identification and characterization of three-dimensional DFAA events

2.2.1. Multi-factor standardized DFAA index

In this study, the calculation of DFAA event characteristics is based on the SDMI time series. The SDMI is constructed based on the joint distribution of the standardized precipitation evapotranspiration index at the response timescale (SPEI-RT) and the one-month standardized soil moisture index (SSMI1). RT denotes the response time (in months) of soil moisture dryness/wetness to meteorological dryness/wetness. For each pixel, the RT is determined as the timescale n at which the Pearson correlation coefficient between the SPEI-n (SPEI at different timescales) and SSMI1 is maximized. This optimal timescale n is then designated as the RT for that pixel. The SDMI is derived by applying the inverse normal transformation to the joint probabilities of drought and flood conditions, which are defined by a copula function as:

$$\mathrm{SDMI}_{\mathrm{drought}} = \varphi^{-1}(p_{\mathrm{drought}}) = \varphi^{-1}[(P(X \le x,\ \ Y \le y)] = \varphi^{-1}[C(u,v)] \quad (1)$$

$$\begin{aligned}\mathrm{SDMI}_{\mathrm{flood}} &= -\varphi^{-1}(p_{\mathrm{flood}}) = -\varphi^{-1}[(P\ \ (X > x,\ \ Y > y)] \\ &= -\varphi^{-1}[1\text{-}u\text{-}v + C(u,\ \ v)]\end{aligned} \quad (2)$$

$$\mathrm{SDMI} = \mathrm{SDMI}_{\mathrm{drought}} \ \le\ 0 \text{ and } \mathrm{SDMI}_{\mathrm{flood}} \ >\ 0 \quad (3)$$

where φ^{-1} is the inverse standard normal distribution function; X and Y represent the univariate thresholds of SPEI-RT and SSMI1, respectively; u and v are their cumulative distribution functions; and $C(u, v)$ is the selected optimal copula function from candidate functions that included the Gaussian copula, t copula, Gumbel copula, Frank copula, and Clayton copula. The SDMI value integrates both components, with SDMI ≤ 0 indicating drought conditions and SDMI > 0 indicating flood conditions.

The multi-factor standardized DFAA index (MSDFI), which is derived from the SDMI series using the following structural formula, is employed specifically to identify the occurrence and type of abrupt transition events. The MSDFI integrates precipitation, evapotranspiration, and soil moisture factors, thereby establishing a stronger linkage with vegetation dynamics. Additionally, the index's multi-time scales can effectively match the lagged response characteristics of vegetation to water stress events. An abrupt alternation between drought and flood conditions in the same pixel, with SDMI values of adjacent units exhibiting significant differences, is defined as drought to flood abrupt alternation or flood to drought abrupt alternation. A brief description of the DFAA identification formula for pixel is as follows:

$$MSDFI = \frac{\mathrm{SDMI}_{i+\mathrm{RT}} - \mathrm{SDMI}_i}{2}\left(1 + \frac{|\mathrm{SDMI}_{i+\mathrm{RT}} - \mathrm{SDMI}_i|}{R}\right)(i\ = 1, 2, \ \ldots, \ n) \quad (4)$$

where SDMI_i is the SDMI value of the i_{th} time series of the pixel, and $\mathrm{SDMI}_{i+\mathrm{RT}}$ is the SDMI value of the $i + \mathrm{RT}_{\mathrm{th}}$ time series of the pixel, R is the deviation between the maximum and minimum SDMI values in the pixel, and n is the length of the sequence. When MSDFI ≥ 0.5, a drought to flood (DTF) event occurs in the pixel; when MSDFI ≤ -0.5, a flood to drought (FTD) event occurs in the pixel.

2.2.2. Identify three-dimensional DFAA events

After identifying the DFAA events, we used a three-dimensional spatiotemporal clustering method to extract the three-dimensional DFAA events. The method is based on the MSDFI index to construct a three-dimensional space, and then spatial density clustering is applied to obtain event clusters. Next, temporal associations between adjacent month events are established, and finally, the complete three-dimensional DFAA events are extracted. The specific steps are as follows (Fig. 2):

1) Construction of a three-dimensional data space. Based on the monthly MSDFI dataset, separate the pixel points where DTF (MSDFI $\ge$ 0.5) and FTD (MSDFI $\le$ -0.5) occur. And then construct the MSDFI spatial maps for DTF and FTD events in chronological order, using longitude, latitude, and time as the three coordinate axes.

2) Extraction of spatial DFAA event clusters. The DFAA events identified through multi-factor integration (precipitation-evapotranspiration-soil moisture) demonstrate spatially dispersed patterns. To spatially associate the identified event pixels within the same month that exhibit either DTF or FTD, implemented the Density-Based Spatial Clustering of Applications with Noise (DBSCAN) spatial clustering method. This approach effectively aggregates the discrete event pixels into coherent clusters. DBSCAN is a density-based clustering algorithm that forms clusters by identifying high-density regions and automatically distinguishes low-density areas as noise (Hahsler et al., 2019). Its core advantages lie in its ability to detect clusters of arbitrary shapes, its robustness to noise, and the fact that it does not require the number of clusters to be predefined (Schubert et al., 2017).

DBSCAN involves two key parameters: eps and minpts. Eps specify the search radius for core points, and minpts defines the minimum number of neighboring pixels required in the region. Different parameter combinations are used to train the DBSCAN model, and the performance of each model is evaluated using the Davies-Bouldin index. A lower Davies-Bouldin index score indicates better clustering performance. Therefore, the parameter combination with the lowest Davies-Bouldin index score was selected as the optimal parameter choice for spatial clustering.

3) Temporal connection of DFAA event clusters. The overlapping area between event clusters of adjacent months is used as the threshold for temporal connection of events. In this study, two event clusters are merged if their overlapping area exceeds $A_0 = 1.5$ % of the study area (approximately 58 grids). This threshold selection follows established practices in previous studies. The pioneering work by Wang et al. (2011) conducted sensitivity tests across different thresholds (ranging from 25,000 km^2 to 200,000 km^2) and identified 150,000 km^2 (approximately 1.5 % of China's land area) as an optimal balance. Subsequent research by Xu et al. (2015) and other scholars (e.g., (Liu et al., 2019; Luo et al., 2024)) has consistently demonstrated that 1.5–1.6 % of the study area serves as a robust threshold.

2.2.3. Characteristic variables of three-dimensional DFAA events

This study defines the duration, area, intensity, spatiotemporal centroid, and migration direction of events to describe the

Table 1
Data and indicators used in this study.

Data type	Data sources
Meteorological data	China Meteorological Forcing Dataset (CMFD) (https://data.tpdc.ac.cn)
Soil moisture data	European Centre for Medium-Range Weather Forecasts (ECMWF) (https://cds.climate.copernicus.eu)
Net Primary Production (NPP), Fractional vegetation cover (FVC)	Global Land Surface Satellite (GLASS) products (https://www.glass.umd.edu)
Normalized difference vegetation index (NDVI)	Peking University Global Inventory Modeling and Mapping Studies NDVI (PKU GIMMS NDVI) dataset (https://zenodo.org/records/8253971)
Land use data	Annual 30-m Land Cover Dataset of China (https://zenodo.org/records/4417810)
Digital elevation model (DEM)	Resource and environment science and data center. (https://www.resdc.cn)

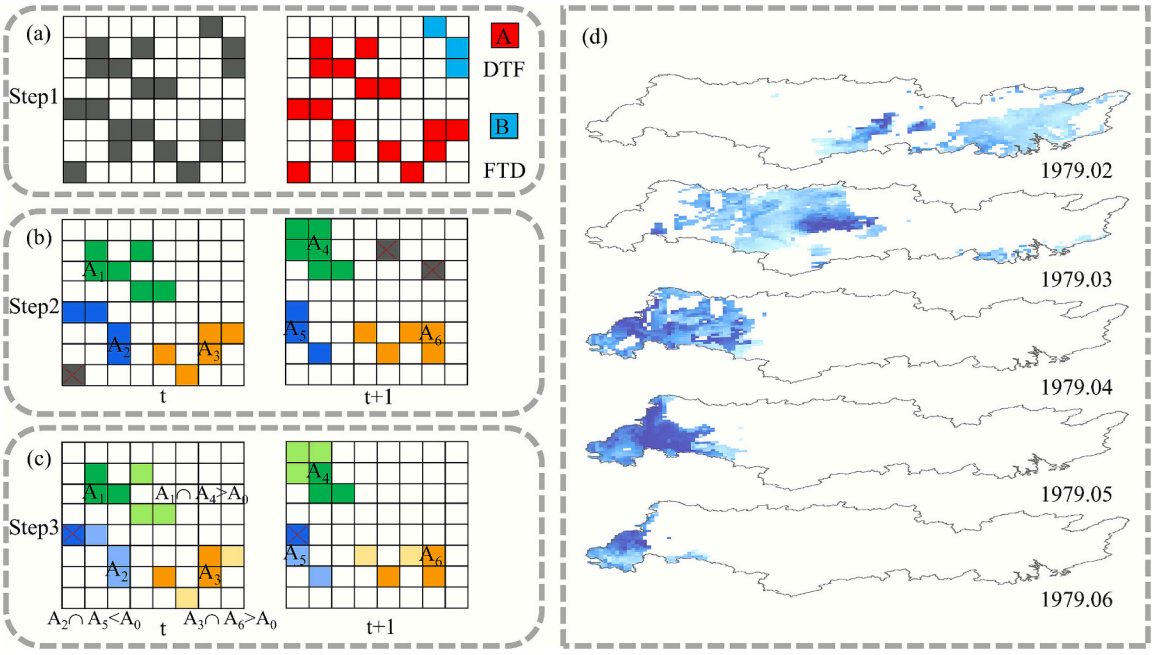


Fig. 2. Three-dimensional identification process of DFAA events. (a) Separation of DTF and FTD events. (b) Clustering of spatial pixels. (c) Overlap validation. (d) Event extraction demonstration (taking the 1979 DTF event as an example).

characteristics of three-dimensional DFAA events.

Duration (D, in months) is defined as the number of consecutive months during which the DFAA event migrates, that is, the height of the three-dimensional DFAA event, as well as the number of months of drought/flood events before and after the DFAA event (*DD/FD*, months).

Affected area (A, in km^2) is defined as the affected area during a DFAA event, which is the maximum projected area of the three-dimensional DFAA event continuum on a coordinate plane. The Affected Area Ratio (*AR*, %) is the ratio of the affected area to the total area of the region.

$$A = N \times A\ (x,\ y) \tag{5}$$

$$AR = \frac{A}{A_{\text{total}}} \times 100\% \tag{6}$$

where N is the total number of grid cells affected by the projection of the DFAA event, x and y represent the longitude and latitude of the grid cells affected by the DFAA event, $A\ (x,\ y)$ is the area of a single grid cell, and A_{total} is the total area of the region.

The intensity of the DFAA event is defined as the intensity of the drought/flood (*DI/FI*) and the intensity term of alternation (*IA*).

$$DI/FI = \frac{DS/FS}{A \times DD/FD} \tag{7}$$

$$DS/FS = \sum_x \sum_y \left(|\text{SDWI}(x,\ y)| - S_0\right) \tag{8}$$

$$IA = \frac{\sum_x \sum_y \left(|\text{SDWI}_{D/F}(x,\ y)| + |\text{SDWI}_{F/D}(x,\ y)|\right)}{2\ A} \tag{9}$$

where *DS/FS* represent drought severity and flood severity, respectively, defined as the cumulative sum of values beyond the 0.5 threshold during the drought or flood period. *DI/FI* denote drought intensity and flood intensity, respectively, and are calculated as the ratio of the corresponding severity to the duration of the event, SDWI $(x,\ y)$ is the index value of the drought/flood event of the DFAA event for the grid cell $(x\ ,\ y)$, $S_0 = 0.5$, $\text{SDWI}_{D/F}$ is the index value of the last month of the drought/flood event before the occurrence of the DFAA event for the grid cell $(x,\ y)$, and $\text{SDWI}_{F/D}$ is the index value of the first month of the flood/drought event after the occurrence of the DFAA event for the grid cell $(x,\ y)$.The calculation process for duration and intensity is shown in Fig.3.

The spatiotemporal centroid of the DFAA event (X_c, Y_c, T_c) characterizes the central location of the event. It is calculated using the weighted average of the MSDFI to determine the spatiotemporal centroid of the three-dimensional DFAA event.

$$\begin{aligned} X_c &= \frac{\sum_x \sum_y (MSDFI(x,y) \bullet x)}{\sum_x \sum_y MSDFI(x,y)}, \\ Y_c &= \frac{\sum_x \sum_y (MSDFI(x,y) \bullet y)}{\sum_x \sum_y MSDFI(x,y)}, \\ T_c &= \frac{\sum_x \sum_y (MSDFI(x,y) \bullet d)}{\sum_x \sum_y MSDFI(x,y)} \end{aligned} \tag{10}$$

where $MSDFI\ (x,\ y)$ is the DFAA index value of the grid cell $(x,\ y)$, and d is the month in which the DFAA event occurs for the grid cell $(x,\ y)$.

The migration direction of DFAA event is defined as the direction of

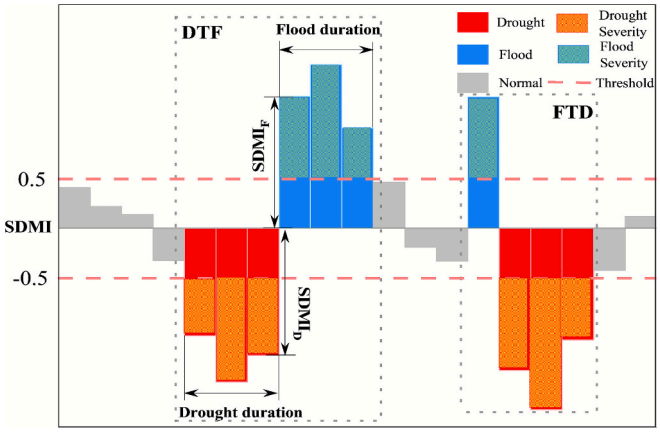


Fig. 3. Schematic diagram of the calculation of the duration and intensity characteristics.

movement from the start to the end of the event, determined based on the centroids of the event's start and end times. If the initial centroid direction of the DFAA event is east and the final direction is west, then the migration direction of the DFAA event is from east to west.

2.3. Assessment of vegetation anomaly to DFAA events

To evaluate vegetation responses to DFAA events, this study analyzes anomalies in vegetation indices within the affected areas during the event period. This approach assesses the ecological impacts of DFAA events on vegetation dynamics by examining spatially and temporally corresponding deviations in vegetation indicators. Vegetation anomalies were calculated as standardized deviations from the long-term mean and standard deviation of each month, effectively removing seasonal trends and isolating DFAA-induced vegetation signals (Li et al., 2022b; Mckee et al., 1993). The formula for calculating the anomaly of the vegetation index is:

$$\Delta D\ (x,\ y,\ d) = \frac{D\ (x,\ y,\ d) - \overline{D\ (x,\ y,\ d)}}{\sigma_{x,\ y,\ d}} \tag{11}$$

where D represents NDVI, FVC, and NPP, x and y represents the longitude and latitude of the grid cell where a DFAA event occurs, d represent the month during which the DFAA event occurs, $D\ (x,\ y,\ d)$ represents the actual vegetation index value for the DFAA event grid cell (x, y) in month d, $\overline{D\ (x,\ y,\ d)}$ and $\sigma_{x,\ y,\ d}$ are the long-term mean value and standard deviation of the vegetation index for the specific month d from 1982 to 2018 during the study period, $\Delta D\ (x,\ y,\ d)$ represents the deviation of the vegetation index in grid cell (x, y) during month d from its long-term mean. A positive or negative value of $\Delta D\ (x,\ y,\ d)$ reflects whether the vegetation index in month-d increased or decreased relative to the long-term average for that month.

2.4. Determination of vegetation response time to DFAA events

Considering the potential lagged response of vegetation indices to DFAA events, this study analyzed the spatial correlation between DFAA events and subsequent vegetation anomalies. Specifically, for each DFAA event month, we extracted the spatial distribution of MSDFI values and compared it with the spatial distribution of vegetation index anomalies at 1–12-month lags. A Spearman rank correlation analysis was conducted between these spatial patterns, specifically comparing the spatial field of MSDFI during the event month with the spatial field of vegetation anomalies at each lagged month. The lag time associated with the maximum spatial correlation coefficient was identified as the vegetation response time for each event (Ding et al., 2020). The most frequently occurring response time during DFAA events was statistically determined as the characteristic lagged response time of the vegetation index to DFAA events. The formula is as follows:

$$R_i = \mathrm{corr}\ (MSDFI,\ \Delta D)\ 1 \le i \le 12 \tag{12}$$

$$R_T = \max\ (R_i)\ 1 \le i \le 12 \tag{13}$$

where: R_i represents the lag time correlation coefficient, with i ranging from 1 to 12, and R_T represents the optimal lag time, which is the lag month i with the highest correlation.

3. Results

3.1. Identified three-dimensional DFAA event

3.1.1. Characteristics of three-dimensional DFAA events

Based on the three-dimensional clustering algorithm, this study identified a total of 99 DFAA events in the Pearl River Basin from 1979 to 2018. Among these events, there were 47 DTF events and 52 FTD events. Tables 2 and 3 showcase the top 10 most severe DTF and FTD events, which are ranked according to their intensity in terms of alternation. Notably, 6 out of the 10 most extreme DTF events occurred before the 2000 s, while 8 of the 10 most intense FTD events took place prior to the 2000 s. This clearly indicates a temporal clustering of severe DFAA events in the earlier decades of the study period.

Fig. 4a illustrates the temporal evolution of duration characteristics for DTF events in the PRB from 1979 to 2018. DTF events predominantly lasted 5–6 months, with 30 % persisting for 5 months and 34 % for 6 months. A temporal shift was observed: during 1979–2004, 5-month durations dominated, whereas post-2004, 6-month durations became more frequent. Fig. 4b shows the evolution for FTD events. The migration durations of FTD events clustered predominantly at 2 months (27 %) and 4 months (33 %), indicating generally shorter durations compared to DTF events. After 2004, the proportion of FTD events with durations $\le$ 4 months increased significantly. Overall, DTF events generally displayed longer migration durations than FTD events. Fig. 4c depicts the mean durations for all event types; the mean values for DTF, FTD, drought, and flood events were 4.7, 4.0, 4.4, and 3.2 months, respectively. Drought events exhibited a distinct intensification pattern, with the average duration escalating from 4.0 months pre-2000 to 4.8 months post-2000, while flood events showed a downward pattern, decreasing from 3.4 months to 2.9 months. A notable pattern emerged: drought became more prolonged, whereas floods exhibited shorter durations.

As shown in Fig. 5, DTF events affected significantly larger areas (mean coverage: 66 %) compared to FTD events (mean coverage: 57 %). Correlation analysis revealed strong positive relationships between migration duration and affected area for both event types (DTF: $r = 0.76$; FTD: $r = 0.81$, $p < 0.05$ for both). This indicates that longer migration durations tend to result in more extensive spatial impacts. Moreover, these findings are consistent with our earlier observation that DTF events generally exhibit longer migration durations than FTD events. The spatiotemporal characteristics displayed in Fig. 6 further show distinct seasonal patterns. Specifically, the spatiotemporal centroid of DTF events mainly occur from February to April, reaching its peak in March, accounting for 57 %. In contrast, the spatiotemporal centroid of FTD events is concentrated from July to September, with August having the highest frequency at 35 %.

3.1.2. Spatial migration of DFAA events

Analysis of spatiotemporal migration patterns reveals distinct characteristics in DTF and FTD events across the PRB (Fig. 7). The spatiotemporal centroid of these two event types predominantly cluster in the central region, yet exhibit systematic east-to-west propagation: 87.2 % of DTF events (41 of 47) demonstrate concentrated westward trajectories, while 75.0 % of FTD events (39 of 52) show similar directional tendency albeit with greater spatial dispersion. The consistent directional bias implies potential predictability in extreme hydroclimatic event propagation across the region.

The study identified representative DFAA events through an integrated assessment of migration duration and alternation intensity, selecting the top-ranked event (highest product value) as the typical case. Event 10 was chosen as the characteristic DTF case (Fig. 8a), exhibiting a 6-month migration duration and maximum affected area of $37.12 \times 104\ km^2$. Originating in January 1987 from the eastern PRB, the event's centroid displayed consistent westward movement, reaching its peak spatial extent ($17.06 \times 104\ km^2$) in April and maximum intensity in May. The spatiotemporal centroid was geolocated at 108.02°E, 24.06°N in April. Remarkably, this event impacted approximately 83.97 % of the entire PRB, with the most prolonged effects concentrated in the western basin.

The analysis selected Event 32 as the representative FTD case (Fig. 8b) based on its the highest overall score. This 7-month duration event initiated in May 2005 in eastern PRB, achieving maximum

Table 2
The top 10 most severe DTF events and their characteristics. The first column 'No.' represents the table is sorted again by the intensity of the events.

No.	Event Time (year/ month)	Event Duration (month)	Area (10^4km^2)	Drought / flood duration (month)	Drought intensity	Flood intensity	intensity term of alternation
1	1987/01 ~ 1987/06	6	37.12	5.4 / 3.9	0.96	0.91	1.56
2	2010/02 ~ 2010/06	5	35.60	5.0 / 3.0	1.40	1.03	1.56
3	2005/01 ~ 2005/06	6	38.71	5.8 / 3.1	1.24	1.19	1.54
4	2009/12 ~ 2010/01	2	7.41	4.8 / 1.9	1.16	1.13	1.53
5	2006/01 ~ 2006/06	6	40.68	6.0 / 3.5	1.02	1.05	1.52
6	1999/02 ~ 1999/06	5	39.98	6.9 / 4.0	1.06	1.03	1.49
7	1980/01 ~ 1980/06	6	39.03	5.2 / 4.0	1.34	0.94	1.48
8	1993/01 ~ 1993/06	6	39.37	5.8 / 4.2	1.01	1.29	1.44
9	1981/01 ~ 1981/05	5	36.39	4.3 / 4.3	0.92	1.02	1.42
10	1998/02 ~ 1998/06	5	16.27	4.1 / 3.1	0.72	1.17	1.40

Table 3
The top 10 most severe FTD events and their characteristics. The first column 'No.' represents the table is sorted again by the intensity of the events.

No.	Event Time (year/ month)	Event Duration (month)	Area (10^4km^2)	Flood / drought duration (month)	Flood intensity	Drought intensity	intensity term of alternation
1	1991/07 ~ 1991/09	3	24.51	2.2 / 4.1	1.08	0.85	1.52
2	1979/07 ~ 1979/10	4	36.65	3.0 / 6.0	1.19	1.27	1.52
3	2010/05 ~ 2010/06	2	14.32	2.6 / 4.8	1.27	0.56	1.52
4	1994/07 ~ 1994/11	5	34.44	4.1 / 3.0	1.34	0.61	1.45
5	1996/07 ~ 1996/12	6	36.45	4.2 / 4.1	1.09	0.87	1.40
6	1998/06 ~ 1998/10	5	38.62	3.1 / 7.4	1.17	1.02	1.39
7	1992/06 ~ 1992/09	4	31.02	3.0 / 6.7	1.15	1.03	1.37
8	2005/05 ~ 2005/11	7	36.37	2.6 / 7.0	1.25	0.98	1.36
9	1988/08 ~ 1988/11	4	37.00	2.3 / 4.6	1.03	0.73	1.34
10	1997/08 ~ 1997/11	4	35.47	4.2 / 3.7	1.22	0.64	1.32

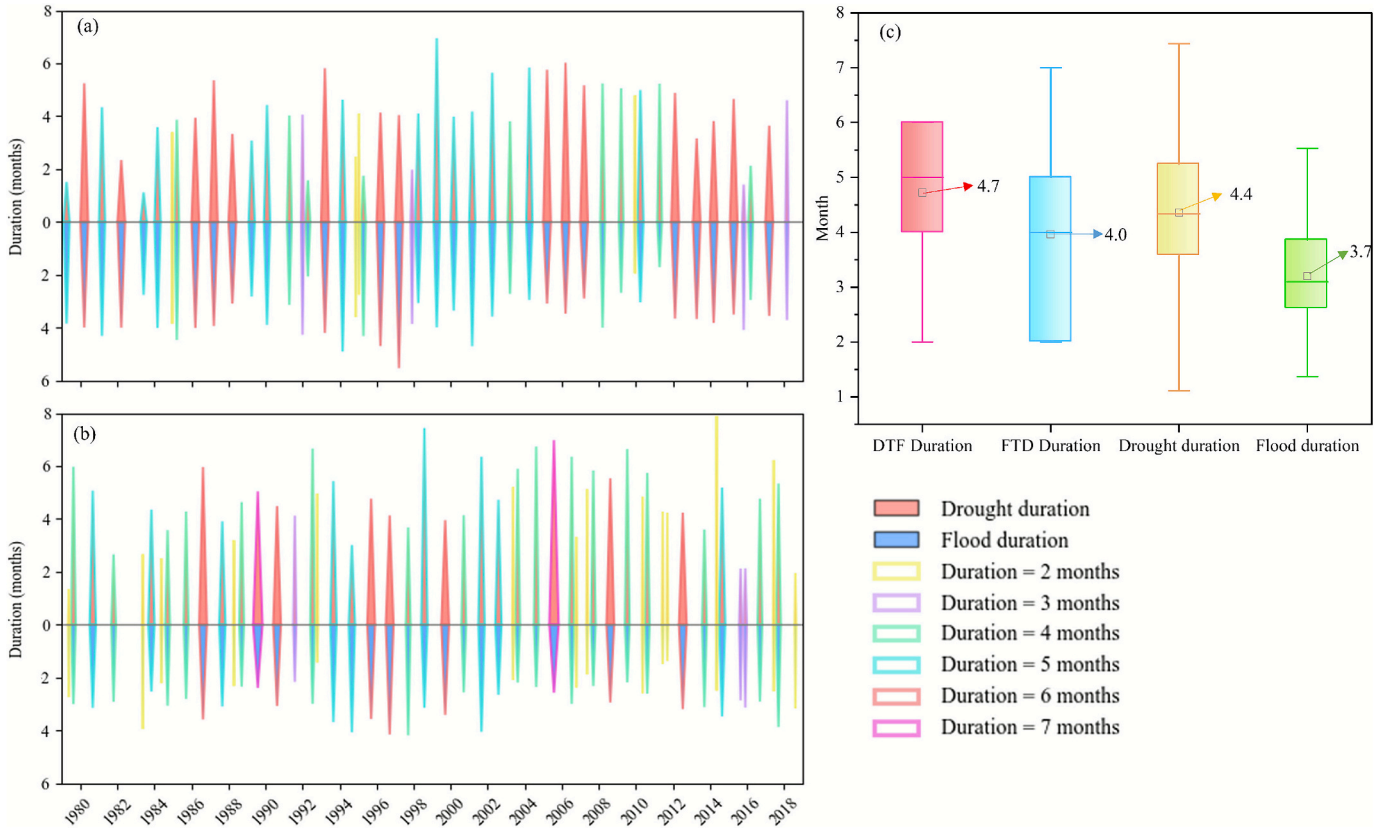


Fig. 4. Duration characteristics of (a) DTF and (b) FTD events showing temporal distributions (drought duration, flood duration, migration duration). (c) Box plots of DFAA event durations (upper/lower quartiles at box ends, horizontal median line, "□" for mean).

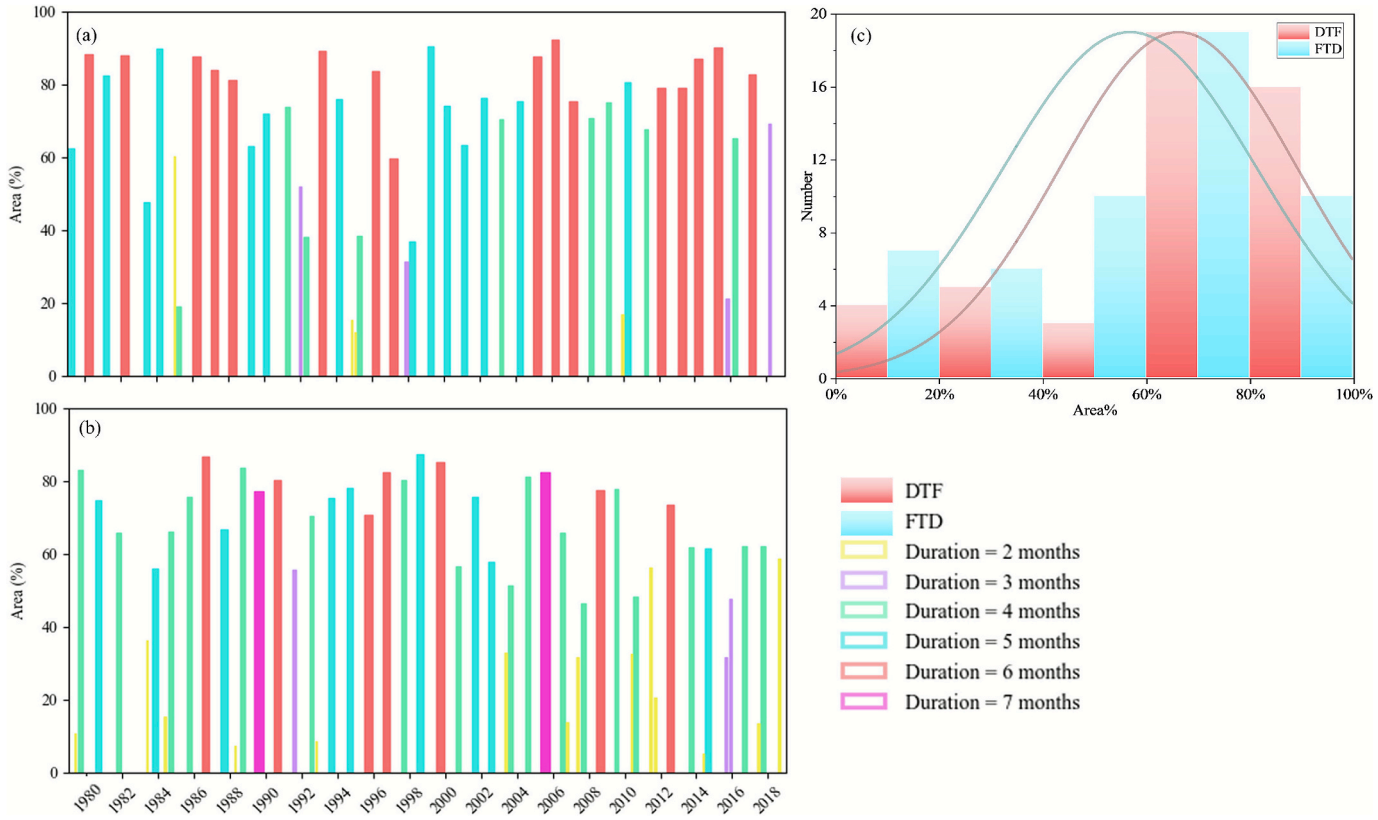


Fig. 5. Temporal distributions of area characteristics for (a) DTF and (b) FTD events. (c) Distribution of DFAA event counts by affected area proportion with fitted normal curve.

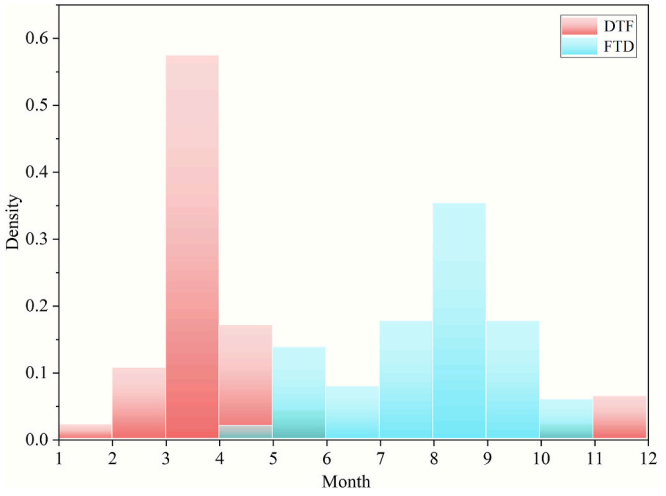


Fig. 6. Monthly density distribution of spatiotemporal centroids for DFAA events (1979–2018).

coverage of 36.37 × 10^4 km^2. Following its westward propagation, the event bifurcated after reaching peak intensity and spatial extent (19.27 × 10^4 km^2) in June. The eastern sector dissipated by September, while the western sector persisted until November. With its spatiotemporal centroid located at 109.52°E, 24.13°N in July, this event affected 82.28 % of the basin, demonstrating particularly dispersed spatial characteristics compared to the DTF case, though similarly showing prolonged impacts in western regions.

3.2. Ecological impact of DFAA events on vegetation

3.2.1. Response of vegetation anomaly to DFAA events

The correlation analysis between MSDFI and vegetation anomalies revealed distinct response patterns of different vegetation indices to DFAA events (Fig. 9). For DTF events, the most frequent response times were 1 month for FVC, 2 months for NDVI, and 7 months for NPP, indicating high sensitivity of FVC/NDVI but low sensitivity of NPP to DTF. In contrast, FTD events led to longer response times. Specifically, it took 6 months for FVC, 8 months for NDVI, and 7 months for NPP. This indicates that suggesting, generally speaking, the sensitivity of vegetation to FTD is weaker. These results demonstrate that DTF events in the PRB can have a rapid impact on vegetation coverage and physiological status, with the effects becoming evident within 1–2 months. In contrast, FTD impacts take a longer time, specifically 6–8 months, to manifest.

3.2.2. DFAA events-induced vegetation variation

Fig. 10 presents the proportion of positive and negative vegetation anomalies during DFAA events, where higher negative values indicate greater areas with vegetation indices below normal growth levels. Analysis reveals distinct patterns between event types: DTF events showed higher mean negative proportions (FVC: 55.41 %, NDVI: 53.96 %, NPP: 42.96 %) compared to FTD events (FVC: 47.84 %, NDVI: 49.06 %, NPP: 18.65 %). Notably, both FVC and NDVI exhibited increasing positive proportions with later event numbers across both DFAA types, suggesting a shift from vegetation suppression to enhancement. In contrast, NPP displayed more complex response dynamics; its negative impact proportions followed a bimodal fluctuation pattern, undergoing two complete cycles of increase and decrease phases during the study period. However, NPP predominantly showed higher-than-normal growth levels during the DFAA events, particularly in FTD events. Collectively, these findings demonstrate that: (1) DTF events have a greater negative impact than FTD events; (2) the suppression effects of

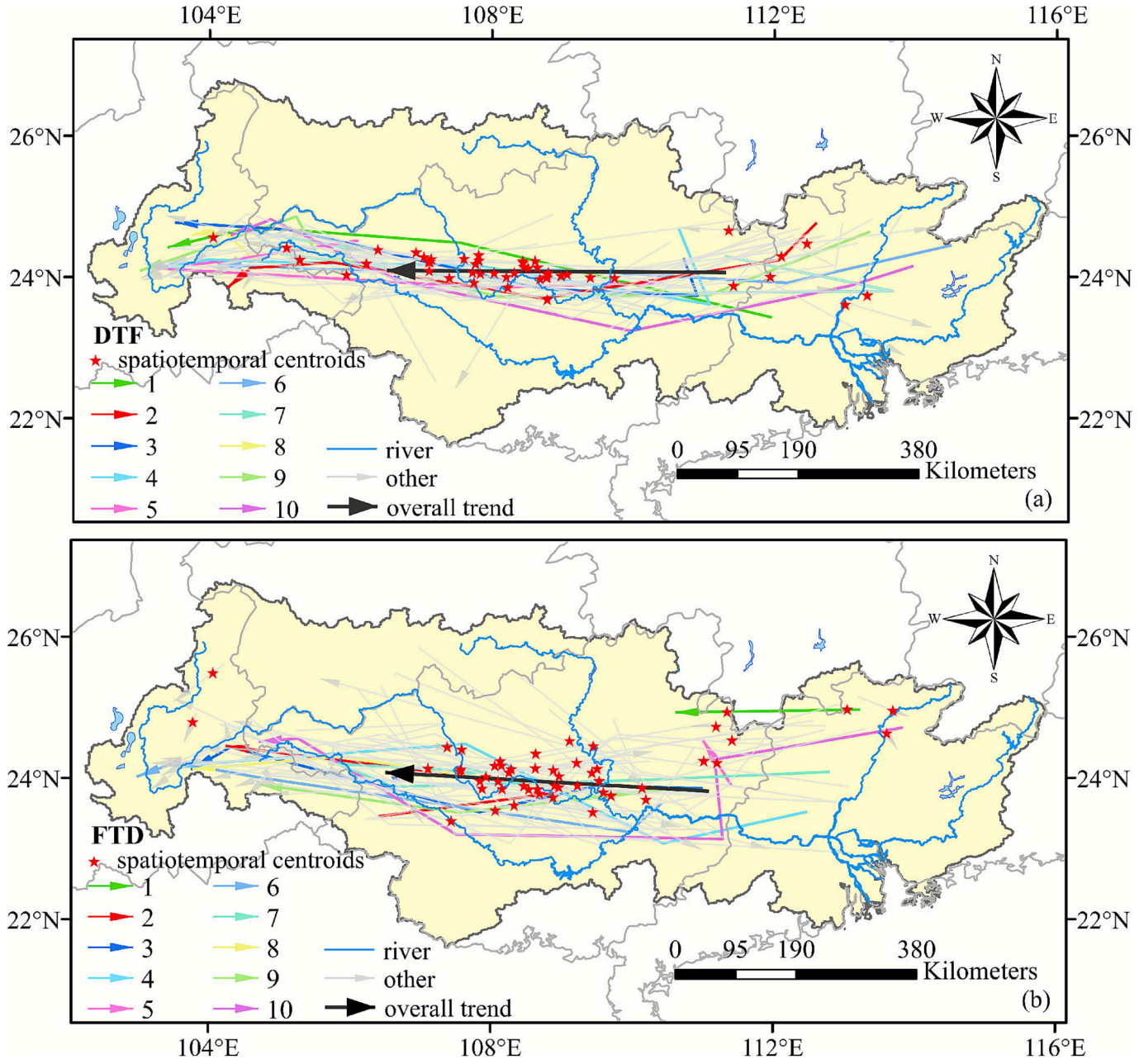


Fig. 7. Migration trajectories of (a) top 10 DTF events and (b) top 10 FTD events ranked by intensity term of alternation, with spatial distribution of spatiotemporal centroids for all events.

DFAA events on vegetation coverage (FVC/NDVI) are weakening; and (3) the negative impacts on productivity (NPP) remain consistently minor.

4. Discussion

4.1. Similarities and differences in DTF and FTD characteristics

This study analyzed the characteristics of DTF and FTD events occurring between 1979 and 2018 in the largest basin of southern China. It has revealed that there are significant differences in their migration duration and spatial extent. Specifically, DTF events exhibited longer migration durations and greater affected areas compared to FTD events. These differences stem from fundamental contrasts in their underlying hydrological mechanisms. For FTD events, the shift from flood to drought is primarily driven by the gradual depletion of soil moisture through evaporation and plant transpiration (Cui et al., 2022; Zhang et al., 2023). This moisture loss process tends to occur relatively uniformly over broad areas, especially in subtropical climates such as the PRB. The relatively rapid rate of moisture loss in these regions contributes to the faster termination of FTD events and consequently shorter transition durations. In contrast, DTF events are typically triggered by localized, intense rainfall systems. The propagation and sequential movement of these rain-producing systems, influenced by atmospheric conditions, act to prolong the DTF event duration and extend their spatial footprint, resulting in prolonged migration durations and broader impacts (Chen et al., 2020; Jiang et al., 2023).

The distinct seasonal timing of DTF and FTD events within the PRB reflects the region's monsoon climate. DTF events occur predominantly during the early-year transition period (February-April), when rainfall interacts with soils that have dried during the winter, triggering localized drought to flood transitions (Deng et al., 2018). In contrast, FTD

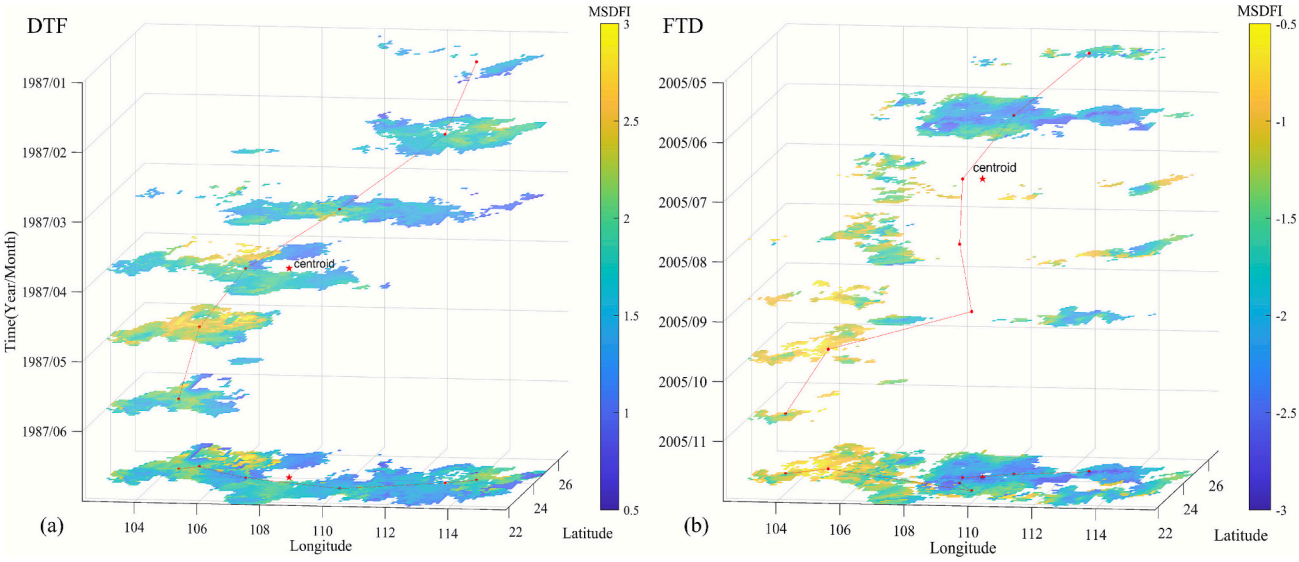


Fig. 8. Three-dimensional migration paths of typical (a) DTF event (Event 10) and (b) FTD event (Event 32).

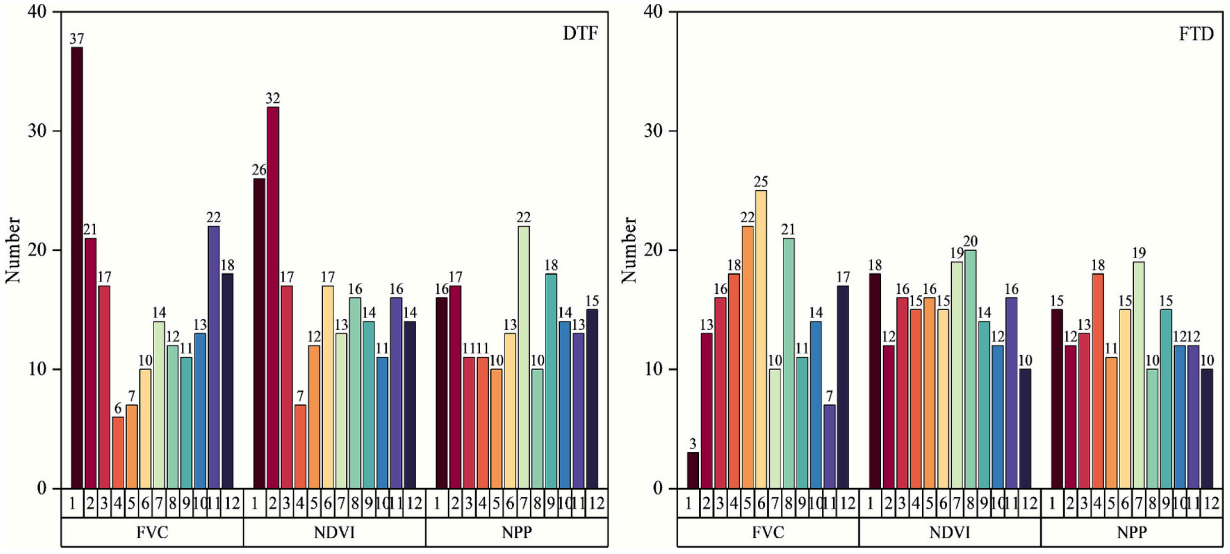


Fig. 9. Distribution of response times for different vegetation indices to DFAA events.

events are concentrated later in the year. During this period, although the rainy season generally persists, the occasional dominance of high-pressure systems can lead to temporary rainfall reduction, accelerating soil moisture depletion and triggering FTD transitions (Wang et al., 2023). This systematic seasonal difference highlights the basin's distinct hydroclimatic drivers: DTF events are primarily initiated by convective rainfall, while FTD events result from intensified atmospheric drought under high temperatures and diminished precipitation—a pattern consistent with previous findings (Li et al., 2024; Qiao et al., 2022; Wang et al., 2025a).

The consistent east-to-west progression of both DTF and FTD events highlights the primary influence of large-scale atmospheric circulation compared to local hydrological factors. This movement pattern is primarily driven by the westward advance of the East Asian monsoon system, which transports moisture inland from the South China Sea, delivering precipitation systems across the basin (Zheng et al., 2017). For DTF events, convective rainfall typically initiates in the eastern coastal zone before moving westward along the monsoon pathway. FTD events show a similar progression, as drought conditions develop following the westward retreat of the monsoon rainfall and the eastward expansion of the subtropical high-pressure system (Gao et al., 2023). Furthermore, the basin's topography, sloping from low-lying eastern areas to higher western elevations, modulates this pattern. It enhances rainfall in the west through orographic effects and creates delayed responses in soil moisture conditions (Lin et al., 2023).

4.2. *Impact of DFAA event on different vegetation indices*

Analysis of vegetation indices (FVC, NDVI, NPP) reveals varying response times to DFAA events, confirming and extending existing knowledge of ecosystem responses. FVC and NDVI respond rapidly to DTF events, typically within 1–2 months, due to their sensitivity to sudden changes like leaf loss or chlorophyll decline. This aligns with findings of a 2-month lag for SIF in the Middle-Lower Yangtze River Basin (Shi et al., 2024). Notably, the weaker sensitivity of NPP to DFAA events stems from the integration of its cumulative carbon assimilation processes, which may be buffered by biochemical inertia and physiological adaptations (Li et al., 2020). In the PRB, prevalent forest cover and carbohydrate reserves likely supported sustained carbon fixation during drought, potentially slowing NPP decline (Sun et al., 2016; Zhou and Zhou, 2021). This temporal offset—where structural changes precede functional responses—emphasizes the critical role of timescale in

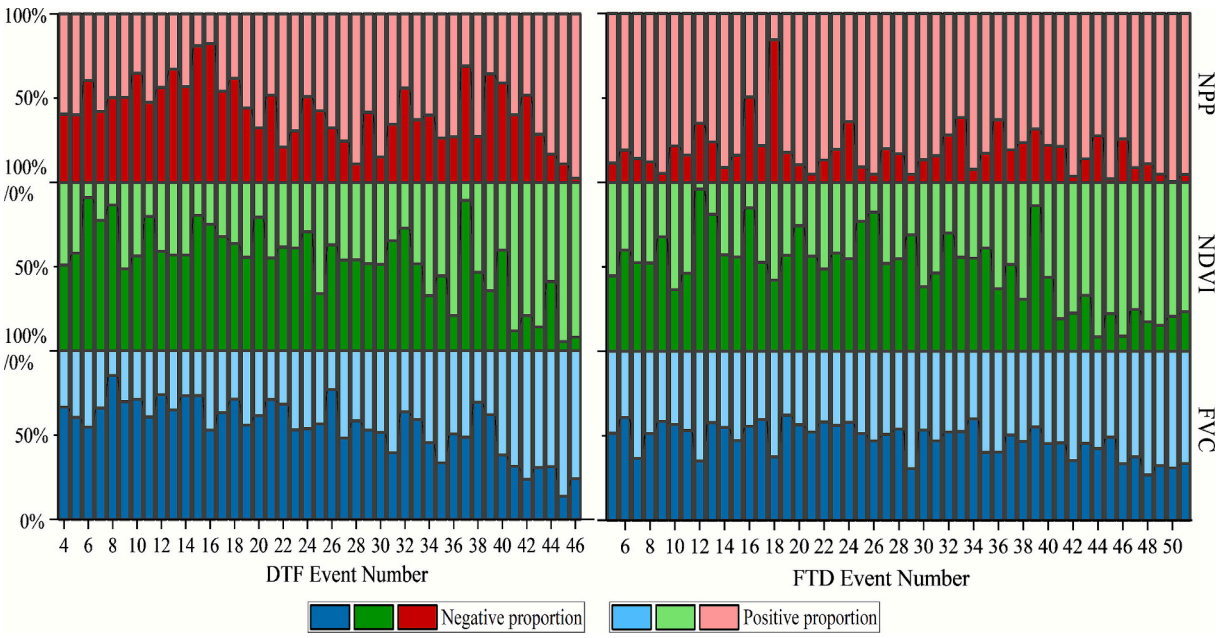


Fig. 10. Impacts of DTF and FTD events on various vegetation indices.

assessing DFAA impacts on ecosystems.

Vegetation generally shows weaker impacts and longer recovery times (exceeding 6 months) following FTD events compared to DTF events. This difference can be explained by seasonal plant adaptations and contrasting environmental conditions. FTD events typically occur during the summer-autumn peak growing season. At this time, vegetation is highly active and can utilize deep root systems to mitigate the effects of sudden soil drying, delaying visible stress in productivity measures. Conversely, DTF events are concentrated in spring and early summer, coinciding with plant growth initiation. During this phase, new foliage and developing root systems are more sensitive to water loss, leading to rapid declines in canopy indicators like NDVI and FVC. Furthermore, the decreasing influence of DFAA events on FVC and NDVI over recent decades aligns with Bai et al. (2024), who reported a significant reduction in FTD severity in the PRB after 2000. This temporal correspondence supports our earlier finding that extreme DFAA events were predominantly concentrated before the 2000 s (Tables 2–3).

An interesting pattern emerged regarding NPP: FTD events generally enhanced NPP in this study, while DTF events showed variable effects. This pattern aligns with observations by Xie et al. (2025) in the China-Pakistan Economic Corridor (CPEC), where FTD events boosted vegetation productivity, but DTF events reduced it. The contrasting responses likely arise from fundamental differences in vegetation type, climate, and soil characteristics between the two regions. The PRB is dominated by subtropical forests with complex canopy structures and deep-rooted trees. These ecosystems exhibit strong resilience to water stress fluctuations (Yin et al., 2024). In contrast, the predominantly arid to semi-arid ecosystems of the CPEC, characterized by shallow-rooted grasses and shrubs, lack comparable adaptive capacity, making them more susceptible to damage from abrupt shifts in water availability.

4.3. Limitations and future prospects

This study introduces a novel approach for tracking the spatial progression of DFAA events and examining their ecological consequences during propagation, providing new insights into DFAA dynamics. However, several limitations warrant acknowledgment. First, the formulaic-based identification method employed constrains the ability to capture the nuanced transition phases between drought and flood conditions. Second, although the overall migration patterns within the PRB were analyzed, the migration trends in other regions remain unexplored, and the underlying driving mechanisms require further investigation. Finally, assessing the ecological impacts of DFAA events remains inherently complex. Current understanding is constrained by limited research on ecosystem responses to DFAA events and the challenge of identifying comprehensive indicators that accurately reflect ecosystem status.

Addressing these limitations warrants targeted future research efforts. First, a more nuanced understanding of DFAA event evolution could be achieved by applying run theory to systematically identify and characterize the distinct drought, transition, and flood phases. Second, elucidating the underlying driving mechanisms behind spatial migration patterns necessitates examining the patterns across diverse basins to establish broader relevance, alongside analyzing the spatiotemporal linkages between migration dynamics and key drivers such as atmospheric circulation patterns and moisture transport pathways. Extending the present method to other climate zones also represents a promising direction, though it would require careful adjustment of index thresholds based on regional characteristics. Finally, comprehensively assessing the ecological impacts calls for developing a multifaceted indicator system to monitor ecosystem condition, facilitating the analysis of phase-specific impacts throughout the DFAA event progression. It is worth noting that the ecological impacts of DFAA events may also vary across different land use types. Future studies conducted over larger and more evenly distributed regions would be valuable to further elucidate these land-use-specific responses.

5. Conclusion

This study developed a novel three-dimensional clustering algorithm to identify DFAA events, characterize their spatiotemporal evolution, and quantify their impacts on vegetation. The main findings are as follows:

(1) The three-dimensional identification method effectively captured the spatiotemporal dynamics of DFAA events in the PRB. A total of 47 DTF and 52 FTD events were detected, with DTF events generally exhibiting longer duration and larger affected areas than FTD events. The spatiotemporal centroids of both event types were predominantly concentrated in the central part of the basin, showing a consistent east-to-west migration tendency.

(2) Divergent ecological impacts were observed between DTF and FTD events. DTF events occurring in spring had a stronger inhibitory effect on vegetation, likely due to the higher susceptibility of newly sprouted leaves. In contrast, FTD events in late summer resulted in relatively weaker impacts, potentially because mature vegetation possesses stronger physiological resistance. Canopy indicators (FVC/NDVI) responded rapidly to DTF events, whereas productivity (NPP) showed a lagged response of up to 7 months for both event types. The inhibitory effect on vegetation cover diminished over time, while NPP primarily showed positive responses. (3) The three-dimensional framework proposed in this study provides an effective tool for analyzing the complete life cycle of DFAA events, identifying their propagation paths, and assessing multi-faceted vegetation impacts. The methodology offers insights for watershed water resource management and ecological conservation, and can be extended to other regions to investigate compound hydrological extremes.

CRediT authorship contribution statement

Xiaoyan Bai: Writing – review & editing, Writing – original draft, Methodology, Funding acquisition, Formal analysis. **Yue Yao:** Writing – original draft, Validation, Software, Data curation. **Jiefeng Wu:** Writing – review & editing, Supervision, Project administration, Funding acquisition, Conceptualization. **Yulei Xie:** Resources, Funding acquisition. **Zhenxing Zhang:** Writing – review & editing.

Declaration of competing interest

The authors declare that they have no known competing financial interests or personal relationships that could have appeared to influence the work reported in this paper.

Acknowledgements

This research was financially supported by the National Natural Science Foundation of China (Grant Nos. 52279008, 52379013, 52222901 and 52379001) and the Natural Science Foundation of Guangdong Province, China (Grant Nos. 2022A1515011648 and 2021A1515010558).

Data availability

The authors do not have permission to share data.

References

Bai, X., Wang, Z., Wu, J., Zhang, Z., Zhang, P., 2024. A novel multivariate multiscale index for drought-flood abrupt alternations: considering precipitation, evapotranspiration, and soil moisture. J. Hydrol. 643. https://doi.org/10.1016/j.jhydrol.2024.132039.

Bi, W., Li, M., Weng, B., Yan, D., Dong, Z., Feng, J., Wang, H., 2023. Drought-flood abrupt alteration events over China. Sci. Total Environ. 875, 162529. https://doi.org/10.1016/j.scitotenv.2023.162529.

Chen, H., Wang, S., Wang, Y., 2020. Exploring abrupt alternations between wet and dry conditions on the basis of historical observations and convection-permitting climate model simulations. J. Geophys. Res. Atmos. 125 (9). https://doi.org/10.1029/2019jd031982.

Chen, Y., Feng, X., Tian, H., Wu, X., Gao, Z., Feng, Y., Piao, S., Lv, N., Pan, N., Fu, B., 2021. Accelerated increase in vegetation carbon sequestration in China after 2010: a turning point resulting from climate and human interaction. Glob. Chang. Biol. 27 (22), 5848–5864. https://doi.org/10.1111/gcb.15854.

Cui, H., Jiang, S., Ren, L., Qin, T., Zhu, Q., Fang, X., Xu, C.-Y., 2025. Identification of drought-flood abrupt alternation by a new non-stationary framework considering natural-social system impacts. J. Hydrol. 654. https://doi.org/10.1016/j.jhydrol.2025.132899.

Cui, H., Jiang, S., Ren, L., Xiao, W., Yuan, F., Wang, M., Wei, L., 2022. Dynamics and potential synchronization of regional precipitation concentration and drought-flood abrupt alternation under the influence of reservoir climate. J. Hydrol.: Reg. Stud. 42. https://doi.org/10.1016/j.ejrh.2022.101147.

Deng, S., Chen, T., Yang, N., Qu, L., Li, M., Chen, D., 2018. Spatial and temporal distribution of rainfall and drought characteristics across the Pearl River basin. Sci. Total Environ. 619–620, 28–41. https://doi.org/10.1016/j.scitotenv.2017.10.339.

Ding, Y., Li, Z., Peng, S., 2020. Global analysis of time-lag and -accumulation effects of climate on vegetation growth. Int. J. Appl. Earth Obs. Geoinf. 92. https://doi.org/10.1016/j.jag.2020.102179.

Feng, K., Wang, Y., Li, Y., Wang, F., Su, X., Zhang, Z., Wu, H., Zhang, G., Li, Y., Wang, X., 2024. Three-dimensional perspective on the characterization of the spatiotemporal propagation from meteorological to agricultural drought. Agric. For. Meteorol. 353. https://doi.org/10.1016/j.agrformet.2024.110048.

Gao, C., Liu, L., Zhang, S., Xu, Y.-P., Wang, X., Tang, X., 2023. Spatiotemporal patterns and propagation mechanism of meteorological droughts over Yangtze River Basin and Pearl River Basin based on complex network theory. Atmos. Res. 292. https://doi.org/10.1016/j.atmosres.2023.106874.

Gao, L., Tao, B., Miao, Y., Zhang, L., Song, X., Ren, W., He, L., Xu, X., 2019. A global data set for economic losses of extreme hydrological events during 1960-2014. Water Resour. Res. 55 (6), 5165–5175. https://doi.org/10.1029/2019wr025135.

Gao, X., Zhao, D., Chen, Z., Zhu, Y., 2022. Changes in abrupt alternations between wet and dry over the Great Lakes Region of Central Asia during the period 1976–2015. J. Hydrol. 613. https://doi.org/10.1016/j.jhydrol.2022.128333.

Hahsler, M., Piekenbrock, M., Doran, D., 2019. dbscan: fast density-based clustering with R. J. Stat. Softw. 91 (1). https://doi.org/10.18637/jss.v091.i01.

He, J., Yang, K., Tang, W., Lu, H., Qin, J., Chen, Y., Li, X., 2020. The first high-resolution meteorological forcing dataset for land process studies over China. Sci. Data 7 (1), 25. https://doi.org/10.1038/s41597-020-0369-y.

Hirabayashi, Y., Kanae, S., Emori, S., Oki, T., Kimoto, M., 2010. Global projections of changing risks of floods and droughts in a changing climate. Hydrol. Sci. J. 53 (4), 754–772. https://doi.org/10.1623/hysj.53.4.754.

Huang, J., Hu, T., Yasir, M., Gao, Y., Chen, C., Zhu, R., Wang, X., Yuan, H., Yang, J., 2019. Root growth dynamics and yield responses of rice (Oryza sativa L.) under drought—Flood abrupt alternating conditions. Environ. Exp. Bot. 157, 11–25. https://doi.org/10.1016/j.envexpbot.2018.09.018.

Huang, S., Tang, L., Hupy, J.P., Wang, Y., Shao, G., 2020. A commentary review on the use of normalized difference vegetation index (NDVI) in the era of popular remote sensing. J. For. Res. 32 (1), 1–6. https://doi.org/10.1007/s11676-020-01155-1.

Jia, K., Yang, L., Liang, S., Xiao, Z., Zhao, X., Yao, Y., Zhang, X., Jiang, B., Liu, D., 2019. Long-term global land surface satellite (GLASS) fractional vegetation cover product derived from MODIS and AVHRR data. IEEE J. Sel. Top. Appl. Earth Obs. Remote Sens. 12 (2), 508–518. https://doi.org/10.1109/jstars.2018.2854293.

Jiang, S., Cui, H., Ren, L., Yan, D., Yang, X., Yuan, S., Liu, Y., Wang, M., Xu, C.-Y., 2023. Will China's Yellow River basin suffer more serious combined dry and wet abrupt alternation in the future? J. Hydrol. 624. https://doi.org/10.1016/j.jhydrol.2023.129871.

Li, D., Ding, Y., Zhou, Z., Wang, T., Wei, R., 2025. The spatiotemporal evolution and propagation characteristics of multiple drought types from a three-dimensional perspective. J. Hydrol. 652. https://doi.org/10.1016/j.jhydrol.2025.132702.

Li, J., Wang, Z., Lai, C., 2020. Severe drought events inducing large decrease of net primary productivity in mainland China during 1982–2015. Sci. Total Environ. 703. https://doi.org/10.1016/j.scitotenv.2019.135541.

Li, M., Cao, S., Zhu, Z., Wang, Z., Myneni, R.B., Piao, S., 2023. Spatiotemporally consistent global dataset of the GIMMS normalized difference vegetation index (PKU GIMMS NDVI) from 1982 to 2022. Earth Syst. Sci. Data 15 (9), 4181–4203. https://doi.org/10.5194/essd-15-4181-2023.

Li, W.-Y., Wen, X., Tan, Q.-F., Tu, Y.-H., Yang, T.-T., Wang, Y.-L., Yu, X.-D., 2022a. Exploring spatio-temporal distribution and evolution of dry-wet alternation using a three-dimensional identification method. J. Hydrol. 612. https://doi.org/10.1016/j.jhydrol.2022.128119.

Li, W., Migliavacca, M., Forkel, M., Denissen, J.M.C., Reichstein, M., Yang, H., Duveiller, G., Weber, U., Orth, R., 2022b. Widespread increasing vegetation sensitivity to soil moisture. Nat. Commun. 13 (1), 3959. https://doi.org/10.1038/s41467-022-31667-9.

Li, X., Yuan, C., Sun, T., Fan, H., 2024. Identifying the spatiotemporal patterns of drought-flood alternation based on IMERG product in the humid subtropical Poyang Lake basin, China. J. Hydrol.: Regional Stud. 54. https://doi.org/10.1016/j.ejrh.2024.101912.

Liang, S., Cheng, J., Jia, K., Jiang, B., Liu, Q., Xiao, Z., Yao, Y., Yuan, W., Zhang, X., Zhao, X., Zhou, J., 2021. The global land surface satellite (GLASS) product suite. Bull. Am. Meteorol. Soc. 102 (2), E323–E337. https://doi.org/10.1175/bams-d-18-0341.1.

Lin, Q., Wu, Z., Zhang, Y., Peng, T., Chang, W., Guo, J., 2023. Propagation from meteorological to hydrological drought and its application to drought prediction in the Xijiang River basin, South China. J. Hydrol. 617. https://doi.org/10.1016/j.jhydrol.2022.128889.

Liu, W., Dong, F., Hu, B.X., You, R., Li, J., Shao, G., 2023. Exploring two-decadal risk variability of drought-flood abrupt alternation in a high-plateau basin. Ecol. Ind. 156. https://doi.org/10.1016/j.ecolind.2023.111106.

Liu, Y., Hu, T., Zhu, R., Li, H., Chen, Q., Jing, P., Mahmoud, A., Wang, Y., Li, X., 2024. Response of rice's hydraulic transport and photosynthetic capacity to drought-flood abrupt alternation. Agric. Water Manage. 303. https://doi.org/10.1016/j.agwat.2024.109023.

Liu, Y., Zhu, Y., Ren, L., Singh, V.P., Yong, B., Jiang, S., Yuan, F., Yang, X., 2019. Understanding the spatiotemporal links between meteorological and hydrological droughts from a three-dimensional perspective. J. Geophys. Res. Atmos. 124 (6), 3090–3109. https://doi.org/10.1029/2018jd028947.

Luo, X., Quang, N.H., Jin, H., Zou, Y., Wu, X., Li, Y., 2024. Probability links between meteorological drought and hydrological drought from a 3D perspective. J. Hydrol.: Reg. Stud. 56. https://doi.org/10.1016/j.ejrh.2024.102001.

Mckee, T.B., Doesken, N.J., Kleist, J.R. 1993 The relationship of drought frequency and duration to time scales.

Muñoz-Sabater, J., Dutra, E., Agustí-Panareda, A., Albergel, C., Arduini, G., Balsamo, G., Boussetta, S., Choulga, M., Harrigan, S., Hersbach, H., Martens, B., Miralles, D.G., Piles, M., Rodríguez-Fernández, N.J., Zsoter, E., Buontempo, C., Thépaut, J.-N., 2021. ERA5-Land: a state-of-the-art global reanalysis dataset for land applications. Earth Syst. Sci. Data 13 (9), 4349–4383. https://doi.org/10.5194/essd-13-4349-2021.

Nie, W., She, D., Xia, J., 2025. Five-century monthly streamflow reconstruction of the upper brahmaputra river reveals historically frequent and intense drought-flood abrupt alternation events. J. Hydrol. 658. https://doi.org/10.1016/j.jhydrol.2025.133195.

Qian, L., Meng, H., Chen, X., Tang, R., 2023. Evaluating agricultural drought and flood abrupt alternation: a case study of cotton in the middle-and-lower Yangtze River, China. Agric. Water Manage. 283. https://doi.org/10.1016/j.agwat.2023.108313.

Qiao, Y., Xu, W., Meng, C., Liao, X., Qin, L., 2022. Increasingly dry/wet abrupt alternation events in a warmer world: observed evidence from China during 1980–2019. Int. J. Climatol. 42 (12), 6429–6440. https://doi.org/10.1002/joc.7598.

Rahmani, F., Fattahi, M.H., 2023. Investigation of alterations in droughts and floods patterns induced by climate change. Acta Geophys. https://doi.org/10.1007/s11600-023-01043-2.

Ren, J., Wang, W., Wei, J., Li, H., Li, X., Liu, G., Chen, Y., Ye, S., 2023. Evolution and prediction of drought-flood abrupt alternation events in Huang-Huai-Hai River Basin, China. Sci. Total Environ. 869, 161707. https://doi.org/10.1016/j.scitotenv.2023.161707.

Rezvani, R., RahimiMovaghar, M., Na, W., Najafi, M.R., 2023. Accelerated lagged compound floods and droughts in northwest North America under 1.5 °C – 4 °C global warming levels. J. Hydrol. 624. https://doi.org/10.1016/j.jhydrol.2023.129906.

Schubert, E., Sander, J., Ester, M., Kriegel, H.P., Xu, X., 2017. DBSCAN revisited, revisited. ACM Trans. Database Syst. 42 (3), 1–21. https://doi.org/10.1145/3068335.

Shan, L., Zhang, L., Song, J., Zhang, Y., She, D., Xia, J., 2018. Characteristics of dry-wet abrupt alternation events in the middle and lower reaches of the Yangtze River Basin and the relationship with ENSO. J. Geog. Sci. 28 (8), 1039–1058. https://doi.org/10.1007/s11442-018-1540-7.

Shi, W., Huang, S., Liu, D., Huang, Q., Han, Z., Leng, G., Wang, H., Liang, H., Li, P., Wei, X., 2021. Drought-flood abrupt alternation dynamics and their potential driving forces in a changing environment. J. Hydrol. 597. https://doi.org/10.1016/j.jhydrol.2021.126179.

Shi, W., Huang, S., Zhang, K., Liu, B., Liu, D., Huang, Q., Fang, W., Han, Z., Chao, L., 2022. Quantifying the superimposed effects of drought-flood abrupt alternation stress on vegetation dynamics of the Wei River Basin in China. J. Hydrol. 612. https://doi.org/10.1016/j.jhydrol.2022.128105.

Shi, X., Yang, Y., Yuan, Z., Ding, H., Zhang, Y., Chen, J., Shi, M., 2024. Integrating SWAP and SIF anomaly to assess the responses of vegetation to the drought-flood abrupt alternation in the middle and lower reaches of the Yangtze River basin, China. J. Hydrol.: Regional Stud. 52. https://doi.org/10.1016/j.ejrh.2024.101726.

Su, J., Ding, Y., Liu, Y., Wang, J., Zhang, Y., 2024. China is suffering from fewer but more severe drought to flood abrupt alternation events. Weather Clim. Extremes 46. https://doi.org/10.1016/j.wace.2024.100737.

Sun, B., Zhao, H., Wang, X., 2016. Effects of drought on net primary productivity: roles of temperature, drought intensity, and duration. Chin. Geogr. Sci. 26 (2), 270–282. https://doi.org/10.1007/s11769-016-0804-3.

Tabari, H., Hosseinzadehtalaei, P., Thiery, W., Willems, P., 2021. Amplified drought and flood risk under future socioeconomic and climatic change. Earth's Future 9 (10). https://doi.org/10.1029/2021ef002295.

Tan, X., Wu, X., Huang, Z., Fu, J., Tan, X., Deng, S., Liu, Y., Gan, T.Y., Liu, B., 2023. Increasing global precipitation whiplash due to anthropogenic greenhouse gas emissions. Nat. Commun. 14 (1). https://doi.org/10.1038/s41467-023-38510-9.

Tu, X., Pang, W., Chen, X., Lin, K., Liu, Z., 2022. Limitations and improvement of the traditional assessment index for drought-wetness abrupt alternation. Shuikexue Jinzhan. 33 (4), 592–601. https://doi.org/10.14042/j.cnki.32.1309.2022.04.007.

Wang, A., Lettenmaier, D.P., Sheffield, J., 2011. Soil moisture drought in China, 1950–2006. J. Clim. 24 (13), 3257–3271. https://doi.org/10.1175/2011jcli3733.1.

Wang, F., Lai, H., Wang, Z., Men, R., Li, Y., Jiang, Y., Feng, K., Tian, Q., Du, X., Qu, Y., 2024a. Dynamic relationships and propagation characteristics between meteorological drought and vegetation drought based on a three-dimensional identification algorithm. Global Planet. Change 240. https://doi.org/10.1016/j.gloplacha.2024.104535.

Wang, J., Rong, G., Li, K., Zhang, J., 2021a. Analysis of characteristics of dry–wet events abrupt alternation in Northern Shaanxi, China. Water. 13 (17). https://doi.org/10.3390/w13172384.

Wang, L., Guo, S., Wang, J., Chen, Y., Qiu, H., Zhang, J., Wei, X., 2024b. A novel multi-scale standardized index analyzing monthly to sub-seasonal drought-flood abrupt alternation events in the Yangtze River basin. J. Hydrol. 633. https://doi.org/10.1016/j.jhydrol.2024.130999.

Wang, R., Li, X., Zhang, Q., Cheng, J., Li, J., Zhang, D., Liu, Y., 2023. Projection of drought-flood abrupt alternation in a humid subtropical region under changing climate. J. Hydrol. 624. https://doi.org/10.1016/j.jhydrol.2023.129875.

Wang, S., Jiang, R., Zhao, Y., Xie, J., Cheng, S., Wang, L., Lu, X., 2025a. Quantifying the drought-flood abrupt alternation events over Wei River Basin: dynamic evolution characteristics, driving factors and inherent mechanism. Atmos. Res. 323. https://doi.org/10.1016/j.atmosres.2025.108185.

Wang, Y., Fu, B., Liu, Y., Li, Y., Feng, X., Wang, S., 2021. Response of vegetation to drought in the Tibetan Plateau: elevation differentiation and the dominant factors. Agric. For. Meteorol. 306. https://doi.org/10.1016/j.agrformet.2021.108468.

Wang, Z., Chen, W., Piao, J., Cai, Q., Chen, S., Xue, X., Ma, T., 2025b. Synergistic effects of high atmospheric and soil dryness on record-breaking decreases in vegetation productivity over Southwest China in 2023. npj Clim. Atmos. Sci. 8 (1). https://doi.org/10.1038/s41612-025-00895-3.

Wu, Z., Li, J., He, J., Jiang, Z., 2006. Large-scale atmospheric singularities and summer long-cycle droughts-floods abrupt alternation in the middle and lower reaches of the Yangtze River. Chin. Sci. Bull. 51 (16), 2027–2034. https://doi.org/10.1007/s11434-006-2060-x.

Xie, L., Li, Y., Zhang, Z., Siddique, K.H.M., Song, X., 2025. Exploring the combined effects of drought and drought-flood abrupt alternation on vegetation using interpretable machine learning model and r-vine copula function. Agric. For. Meteorol. 370. https://doi.org/10.1016/j.agrformet.2025.110568.

Xiong, Q., Zhong, L., Du, J., Zhu, C., Peng, X., He, X., Fu, J., Ouyang, L., Bian, J., Hu, L., Sun, X., Xu, J., Zhou, D., Cai, Y., Fu, H., He, H., Chen, X., 2020. Ribosome profiling reveals the effects of nitrogen application translational regulation of yield recovery after abrupt drought-flood alternation in rice. Plant Physiol. Biochem. 155, 42–58. https://doi.org/10.1016/j.plaphy.2020.07.021.

Xiong, Q.Q., Shen, T.H., Zhong, L., Zhu, C.L., Peng, X.S., He, X.P., Fu, J.R., Ouyang, L.J., Bian, J.M., Hu, L.F., Sun, X.T., Xu, J., Zhou, H.Y., He, H.H., Chen, X.R., 2019. Comprehensive metabolomic, proteomic and physiological analyses of grain yield reduction in rice under abrupt drought-flood alternation stress. Physiol. Plant. 167 (4), 564–584. https://doi.org/10.1111/ppl.12901.

Xu, K., Yang, D., Yang, H., Li, Z., Qin, Y., Shen, Y., 2015. Spatio-temporal variation of drought in China during 1961–2012: a climatic perspective. J. Hydrol. 526, 253–264. https://doi.org/10.1016/j.jhydrol.2014.09.047.

Yan, K., Gao, S., Chi, H., Qi, J., Song, W., Tong, Y., Mu, X., Yan, G., 2022. Evaluation of the Vegetation-Index-based Dimidiate Pixel Model for Fractional Vegetation Cover Estimation. IEEE Trans. Geosci. Remote Sens. 60, 1–14. https://doi.org/10.1109/tgrs.2020.3048493.

Yang, G., Chang, J., Wang, Y., Guo, A., Zhang, L., Zhou, K., Wang, Z., 2024. Understanding drought propagation through coupling spatiotemporal features using vine copulas: a compound drought perspective. Sci. Total Environ. 921. https://doi.org/10.1016/j.scitotenv.2024.171080.

Yang, H., Ma, F., Yuan, X., Ji, P., Li, C., 2025. Vegetation greening accelerated the propagation from meteorological to soil droughts in the Loess Plateau from a three-dimensional perspective. J. Hydrol. 650. https://doi.org/10.1016/j.jhydrol.2024.132522.

Yang, J., Huang, X., 2021. The 30 m annual land cover dataset and its dynamics in China from 1990 to 2019. Earth Syst. Sci. Data 13 (8), 3907–3925. https://doi.org/10.5194/essd-13-3907-2021.

Yang, P., Zhang, S., Xia, J., Zhan, C., Cai, W., Wang, W., Luo, X., Chen, N., Li, J., 2022. Analysis of drought and flood alternation and its driving factors in the Yangtze River Basin under climate change. Atmos. Res. 270. https://doi.org/10.1016/j.atmosres.2022.106087.

Yin, S., Du, H., Mao, F., Li, X., Zhou, G., Xu, C., Sun, J., 2024. Spatiotemporal patterns of net primary productivity of subtropical forests in China and its response to drought. Sci. Total Environ. 913. https://doi.org/10.1016/j.scitotenv.2023.169439.

Yu, T., Sun, R., Xiao, Z., Zhang, Q., Liu, G., Cui, T., Wang, J., 2018. Estimation of global vegetation productivity from global land surface satellite data. Remote Sens. (Basel) 10 (2). https://doi.org/10.3390/rs10020327.

Yu, Y., Fu, J., Liu, B., Huang, Z., Tan, X., 2024. Assessing spatiotemporal variation in dry-wet abrupt alternation using an improved process-based approach. J. Hydrol.: Reg. Stud. 54. https://doi.org/10.1016/j.ejrh.2024.101859.

Zhang, Q., Li, J., Gu, X., Shi, P., 2018. Is the Pearl River basin, China, drying or wetting? Seasonal variations, causes and implications. Global Planet. Change 166, 48–61. https://doi.org/10.1016/j.gloplacha.2018.04.005.

Zhang, Q., Wang, Y., 2022. Distribution of hazard and risk caused by agricultural drought and flood and their correlations in summer monsoon–affected areas of China. Theor. Appl. Climatol. 149 (3–4), 965–981. https://doi.org/10.1007/s00704-022-04093-6.

Zhang, Y., You, Q., Ullah, S., Chen, C., Shen, L., Liu, Z., 2023. Substantial increase in abrupt shifts between drought and flood events in China based on observations and model simulations. Sci. Total Environ. 876, 162822. https://doi.org/10.1016/j.scitotenv.2023.162822.

Zhao, D., Deng, S., Zhang, J., 2022. Spatiotemporal characteristics of dry-wet abrupt alternation events in China during 1960–2018. Int. J. Climatol. 42 (16), 9612–9625. https://doi.org/10.1002/joc.7850.

Zhao, Y., Weng, Z., Chen, H., Yang, J., 2020. Analysis of the evolution of drought, flood, and drought-flood abrupt alternation events under climate change using the daily SWAP index. Water 12 (7). https://doi.org/10.3390/w12071969.

Zheng, Y., He, Y., Chen, X., 2017. Spatiotemporal pattern of precipitation concentration and its possible causes in the Pearl River basin, China. J. Cleaner Prod. 161, 1020–1031. https://doi.org/10.1016/j.jclepro.2017.06.156.

Zhou, W., Liu, D., Zhang, J., Jiang, S., Xing, S., Wang, J., Cheng, Y., Chen, N., 2023. Identification and frequency analysis of drought–flood abrupt alternation events using a daily-scale standardized weighted average of the precipitation index. Front. Environ. Sci. 11. https://doi.org/10.3389/fenvs.2023.1142259.

Zhou, Y., Zhou, P., 2021. Decline in net primary productivity caused by severe droughts: evidence from the Pearl River basin in China. Hydrol. Res. 52 (6), 1559–1576. https://doi.org/10.2166/nh.2021.061.

Zhu, R., Wu, F., Zhou, S., Hu, T., Huang, J., Gao, Y., 2020. Cumulative effects of drought–flood abrupt alternation on the photosynthetic characteristics of rice. Environ. Exp. Bot. 169. https://doi.org/10.1016/j.envexpbot.2019.103901.